Available online at www.sciencedirect.com
SCIENCE DIRECT
Polymer 46 (2005) 5556–5568
polymer
www.elsevier.com/locate/polymer

Polymer thin film photodegradation and photochemical crosslinking: FT-IR imaging, evanescent waveguide spectroscopy, and QCM investigations

Mitchel D. Millan, Jason Locklin, Timothy Fulghum, Akira Baba, Rigoberto C. Advincula*

Department of Chemistry, University of Houston, 136 Fleming Building, Houston, TX 77204-5003, USA

Received 3 January 2005; received in revised form 9 May 2005; accepted 10 May 2005

Abstract

Photodegradation and photocrosslinking of benzophenone blended polystyrene (PS) thin films were investigated primarily using Fourier transform infrared (FT-IR) imaging, evanescent waveguide spectroscopy (WS), and quartz crystal microbalance (QCM) methods. The main objective is to observe the changes (spectral and chemical) indicative of these competitive processes in an ultrathin polymer film. This also serves as a model study in the application of combined spectroscopic, optical, and acoustic methods towards understanding crosslinking and degradation phenomena within the same time frame of observation. To induce photocrosslinking, 1,12-dodecanediylbis(oxy-4,1-phenylene)] [bis[phenylmethanone] (2BP12), a small molecule with two benzophenone groups, was blended with PS in solution, spincast onto glass and silicon substrates, and irradiated with ultraviolet light. Photodegradation and benzophenone-mediated crosslinking were observed both directly via functional group spectroscopies and indirectly via their effects on thin film surface properties and morphologies. Atomic force microscopy (AFM) and QCM were used to elucidate local morphology change and mass-uptake kinetics in the presence of O_2 in air, respectively. All results correlated well with the two photoprocesses occurring simultaneously and competitively on these films with the refractive index, thickness, and mass change differing with the presence of 2BP12. Crosslinking was observed to cause an increase in thickness while photodegradation gave a decrease. Both processes resulted in an increase in the refractive index and mass. While various methods have separately identified these observations, this is the first instance that the in situ chemical, optical, and structural dimensionality of the photodegradation and photocrosslinking phenomena in a thin polymer film is correlated within the same time frame of observation.

Keywords: FT-IR imaging; Evanescent waveguide; Photodegradation

1. Introduction

Polysytrene (PS) is one of the most ubiquitous of commercial polymers. Due to the huge variety of its applications, photoinitiated degradation and oxidation in air are important issues. These decomposition processes have been reported to typically occur over the range of 250–400 nm [1], and can be initiated even by ordinary sunlight [2]. According to accepted terminology, photodegradation refers to light-initiated chain scission, crosslinking and other processes under vacuum or inert atmosphere. On the other hand, oxidative photodegradation (or degradative photooxidation) occurs in air and includes, in addition to the processes described above, the formation of various oxygen-containing functional groups such as peroxides or carbonyls. In this work, the term photodegradation will be used in general, and the environment in which occurs will be obvious from context.

Numerous mechanisms for PS photodegradation have been proposed over the years [3], but a totally consistent theory is yet to be agreed upon, due to the complexity of the kinetics and the formation of various photodegradation products. An accepted classical mechanism [1,4] for PS degradation under ultraviolet (UV) light is given in Scheme 1. When irradiated at $\lambda < 300$ nm, PS forms the PS radical (Eq. (1)), which in air leads to a peroxyradical, and eventually a PS hydroperoxide (Eq. (2)). The latter photolyzes into an alkoxy radical (Eq. (3)), leading to

* Corresponding author. Tel.: +1 713 743 1760; fax: +1 713 743 1755.
E-mail address: radvincula@uh.edu (R.C. Advincula).

0032-3861/$ - see front matter © 2005 Elsevier Ltd. All rights reserved.
doi:10.1016/j.polymer.2005.05.050

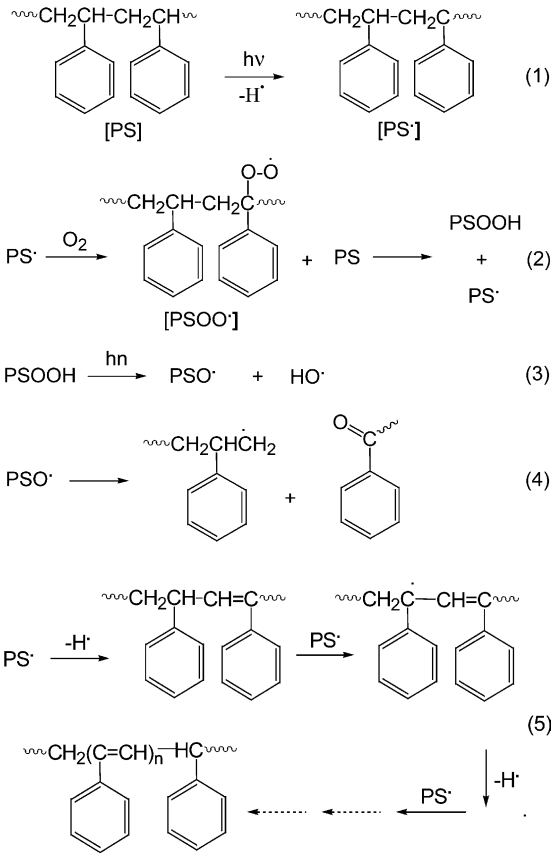

Scheme 1. Mechanism for photodegradation of PS.

chain scission with the formation of shorter chain PS radicals and carbonyl species (Eq. (4)). In addition to chain scission, conjugated alkenes also form in the aliphatic portion of PS through stable polyene radical intermediates (Eq. (5)). Polyene formation (which causes, in addition to other factors, yellowing in degrading PS) is the major decomposition process occurring when PS is irradiated under vacuum.

The mechanism above shows that the reactive PS hydroperoxide is formed upon exposure to atmospheric oxygen. However, the photodegradation process can be initiated by in-chain structural defects [5], such as hydroperoxides formed during the polymerization of styrene and subsequent processing. Mechanistic studies have also been performed using external photoinitiators such as peroxides, benzophenone (BP) [6], and other ketones and aldehydes [7]. Such initiators increase the rate and efficiency of photodegradation by the process below, shown for BP in Scheme 2. BP forms a triplet ketyl radical upon UV irradiation (Eq. (6)), which abstracts a hydrogen from PS (Eq. (7)). The singlet BP radical in the presence of oxygen forms the highly reactive hydroperoxide radical (Eq. (8)). The latter upon reaction with a PS radical produces a PS hydroperoxide (Eq. (9)), which decomposes as discussed above in Eqs. (3)-(4). Kaczmarek and co-workers have shown photoinitiation as the dominant function of BP (and

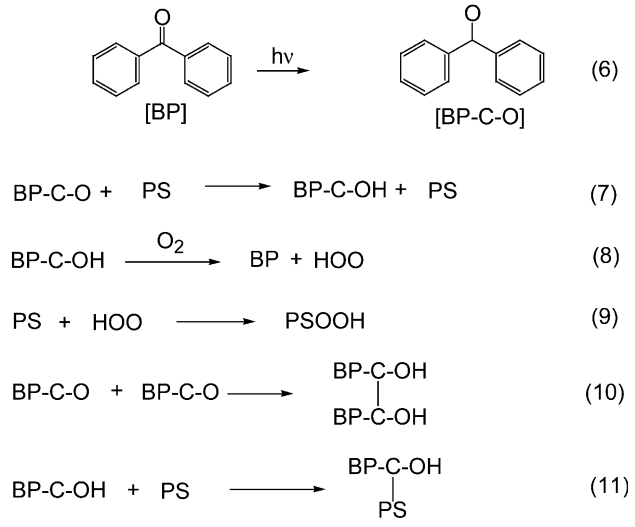

Scheme 2. Initiation of Photodegradation of PS by BP.

other initiators) at relatively low concentration (0.1%) in a PS matrix when irradiated in air [6]. At a higher concentration (0.5%), photodegradation efficiency decreases. This change is due to phase-incompatibility between PS and BP, and decrease in their surface contact. In addition to this, benzopinacol formation from ketyl radical combination (Eq. (10)) competes with the initiation and acceleration of PS degradation. Crosslinking can also become a major process when a singlet BP radical and a PS radical (Eq. (11)) combine although this has not been thoroughly investigated before [8].

1.1. Investigation methods for photodegradation and photocrosslinking

PS degradation processes can be observed by a number of techniques, including thermal and dynamic mechanical analyses. For example, simple viscometric measurements of irradiated films of PS–BP blends [4] show a decrease in viscosity-average molecular weight, M_v, as chain scission occurs at low initiator concentrations. As BP concentration is increased incrementally, M_v eventually increases as crosslinking becomes more pronounced. These physico–mechanical methods are important for analyses of the bulk polymers. Spectroscopic methods are also common, for bulk as well as film samples. Electron spin resonance spectroscopic measurements of PS films irradiated both under vacuum and in air give spectra assigned to the PS radical and the peroxyradical [8]. Pioneering work by Gueskens and co-workers shows IR peaks at 3300–3500 and $\sim$1700 cm^{-1} for hydroperoxide and carbonyl species, respectively [9]. The C=C stretch of degradation polyolefin products is not observed directly in the IR, due to overlap with the strong phenyl ring stretch at 1601 cm^{-1}. However, they have reported these chromophores using UV–vis spectroscopy. While much investigation has been done on bulk samples, only a few detailed studies have focused on thin films using

combined spectroscopic, microscopic, and acoustic methods within the same time frame of observation.

1.2. Analysis techniques for thin films

There is a lot of interest in polymers (including PS) cast as thin films. In this form, many novel applications present themselves for mechanical, optical, and electronic thin film devices and coatings. It is also known that the physical properties of polymers can deviate significantly from those of bulk samples when the film thickness is less than 150–100 nm [10,11]. Therefore, techniques that are sensitive to the physico–chemical processes occurring with ultrathin films are of great interest for structure–property correlation and understanding of phenomena. Thus, we have sought in this work to investigate the analysis of PS photodegradation and photocrosslinking using such methods.

1.2.1. FT-IR imaging

FT-IR Imaging [12] is a technique for obtaining spatially and temporally-resolved chemical and structural information. As such, it can provide a 'still picture' of specific functional groups, e.g. a carbonyl moiety, over a relatively large sample area at specific periods of time. As a non-destructive technique, it has been applied to numerous polymeric systems for observing processes as diverse as oxidation [13], crosslinking [14], and crystallization [15]. Physical blends [16], and dissolution of polymers in various solvents [17] including supercritical CO_2 [18] have also been monitored. The use of synchrotron radiation as the IR source drastically improves spectral quality [19a,b], and new sampling techniques like internal reflection IR imaging (IRIRI) or micro-ATR provide enhanced spatial resolution [19c,d]. Since FT-IR imaging allows real-time observation of chemical changes in functional groups, we have utilized it to observe the photochemical processes in a PS-initiator polymer blend degradation and cross-linking study.

1.2.2. Evanescent waveguide spectroscopy (WS)

WS can be used to determine the thickness and refractive indices of polymer films when deposited on a noble metal surface. Typically, gold (45 nm) is coated on a glass slide, the polymer film is cast on the gold side, and the glass side of the substrate is then put into optical contact with a glass prism using a refractive index matching liquid, using the Kretschmann coupling technique [21].

When the polymer is of sufficient thickness, guided optical waves can propagate in a direction parallel to the substrate plane. These waveguide modes exist subject to the following condition [22]:

$$k_z d = m\pi + \beta_1 + \beta_2 \tag{12}$$

where k_z is the component of the wave vector normal to the substrate plane, and d is the thickness of the polymer film, m is the order of the waveguide mode, and β_i ($i=1,2$) are the phase shifts of the propagating wave at the film boundaries. β_I are dependent on the polarization of light, and are defined by Fresnel formulas.

For very thin layers of polymer, a surface plasmon resonance (SPR) mode ($m=0$) can be observed using p-polarized light. With increased thickness, two possible waveguide modes can be excited depending on the polarization of light: (i) a transverse magnetic (TM) mode under p-polarization, which is sensitive to both the out-of-plane refractive index n_z and the in-plane n_y in the direction of guided wave propagation, and (ii) a transverse electric (TE) mode under s-polarization, sensitive to the in-plane n_x perpendicular to the guided wave direction. When reflectivity (R) is measured versus angle of incidence θ, minima are observed beyond a critical angle θ_c according to the number of modes ($m=$integer) excited. The angle θ of these minima depend on the dielectric constants ε and the thicknesses of the waveguide layers, including the glass, gold, and polymer [23]. The thickness(es) and ε of the gold layer (and any underlying metal) can be determined from SPR data (using the same Kretschmann set-up) by simulating the spectrum of the bare gold-coated substrate using Fresnel calculations. The experimental waveguide spectra can then be fit to generate thickness d and refractive index n ($n^2=\varepsilon$) for the polymer layer. WS can be a powerful tool to determine thickness, optical properties, and even molecular orientation of thin films. For instance, anisotropy in the film can be detected by non-identical values of n_x, n_y, and n_z. Again, a series of spectra periodically obtained can be used to observe changes as a function of time.

1.2.3. Quartz crystal microbalance (QCM)

The QCM is a highly sensitive technique for observing mass changes due to physical or chemical changes occurring in a thin layer of material deposited on a quartz crystal [24]. The piezoelectric properties of the crystal changes with mass adsorption at the interface of the crystal and air, causing a change in the oscillating frequency F_q. The resulting change in frequency ΔF can be used to measure a mass change Δm in the nanogram scale, using the Sauerbrey equation [25], tailored to the parameters in the QCM experiment:

$$\Delta F = \frac{-2F_q^2 \Delta m}{A\sqrt{\rho_q \mu_q}} \tag{13}$$

where F_q is the resonant frequency of the QCM crystal, A is the area of the electrode, ρ_q is the density of quartz (2.65 g/cm^3) and μ_q is the shear modulus of quartz (2.95×10^6 N/cm^2). The values pertinent to our work are $F_q=5$ MHz, and $A=1.227$ cm^2. Plugging in the appropriate values, the change in mass can be determined directly from the equation:

$$\Delta m = -2.17\times10^{-8}\Delta F \text{ (Hz)} \tag{14}$$

This equation is taken to be valid for measurements taken

both in air and in vacuum [26]. By measuring the frequency or mass changes as a function of time, kinetic data can be obtained.

2. Experimental section

2.1. Materials

Polystyrene (average M_w 250,000) was purchased from Acros Organics. All other materials were purchased from Aldrich and used without further purification. All solvents were purchased from EM Science and used without further purification.

2.1.1. Synthesis of 2BP12

[1,12-Dodecanediylbis(oxy-4,1-phenylene)][bis[phenylmethanone], 2BP12 (Scheme 3) was obtained as the secondary product in a published procedure [27] for the synthesis of 4-(12-bromododecyloxy)benzophenone. 4-Hydroxybenzophenone (3.15 g, 15.9 mmol), 1,12-dibromododecane (5.22 g, 15.9 mmol), and potassium carbonate (2.76 g, 20 mmol) were combined in 40 mL acetone in a one-neck flask. The mixture was refluxed overnight and then poured into water, extracted with ether, and dried over magnesium sulfate. Upon removal of solvent, a mixed solid was obtained. Dissolution and recrystallization of the solid yielded 4-(12-bromododecyloxy)benzophenone. Evaporation of the supernatant liquid gave 2.1 g (yield 23.5%) of the desired product 2BP12. ^{1}H NMR (300 MHz, $CDCl_3$, ppm) δ 7.82 (d, 4H), 7.75 (d, 4H), 7.56 (dd, 2H), 7.46 (dd, 4H), 6.95 (d, 4H), 4.03 (t, 4H), 1.81 (dt, 4H) 1.47 (m, 4H), 1.31 (m, 12H). ^{13}C NMR (75 MHz, $CDCl_3$, ppm) δ 192.52, 162.84, 138.34, 132.52, 131.79, 129.86, 129.66, 128.13, 122.65, 113.97, 68.24, 29.53, 29.33, 29.10, 25.97.

2.1.2. Substrate preparation

All glass and silicon substrates were cleaned by dipping in piranha solution (30:70 v/v of 30% w/w hydrogen peroxide and 98% w/w sulfuric acid) for at least 30 min, rinsing thoroughly with deionized water (resistivity 18.2 MΩ), purified through a Milli-Q Academic System (Millipore Corporation) with a 0.22 μm Millistack filter. Substrates were then dried with an air-jet, then cleaned with a March Plasmod (March Instruments, Inc.) oxygen plasma cleaner prior to use.

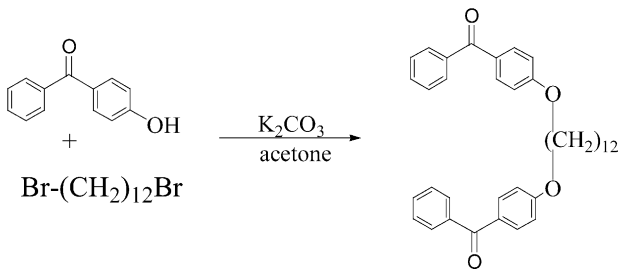

Scheme 3. Synthesis of 2BP12.

2.2. Characterization and instrumentation

2.2.1. UV-irradiation of samples

All irradiation experiments were performed with an Oriel Hg–Xe lamp with a typical power of 100 mW/cm^2 at an average distance of 25 cm from the substrate.

2.2.2. UV–vis spectroscopy

UV–vis spectra were obtained using an Agilent 8453 UV–vis spectrometer. A blend of 50:50 wt% PS:2BP12 was suspended in enough $CHCl_3$ to make a 10% solution, filtered, and spincast on clean glass slides at 1000 rpm for 120 s. This solution and all subsequent ones described below were filtered through 0.2 μM hydrophobic fluoropore (PTFE) filters (Millex, Millipore). All samples were irradiated for specified times, and the absorption spectrum taken after each time increment.

2.2.3. FT-IR spectroscopy and imaging

All spectra and images were obtained using a Digilab Stingray system consisting of a FTS 7000 Step-scan spectrometer and UMA 600 IR Microscope. IR images were obtained using a 32×32 array MCT-FPA detector, covering a sample area of 176×176 μm^2 in transmission mode. All images were taken with a nominal spectral resolution of 8 cm^{-1} and an undersampling ratio of four. A typical imaging experiment used 5000 scans with a total acquisition time of about 30 min. All images were processed using the included software Win-IR Pro 3.4. For PS:2BP12 irradiated in solution, a blend of 50:50 wt% PS:2BP12 was suspended in enough $CHCl_3$ to make 2 mL of a 10% solution in a 1 cm quartz cuvette. This concentration was necessary in order to attenuate the spectral data based on previous optimization studies. With constant stirring, the mixture was irradiated through the cuvette for specified times. A small aliquot was then obtained after each time increment, and spincast on silicon wafers at 1000 rpm for 120 s. For PS:2BP12 irradiated as thin films, a blend of 50:50 wt% PS:2BP12 was suspended in enough $CHCl_3$ to make a 10% solution, filtered, and spincast on a clean silicon wafer at 1000 rpm for 120 s.

2.2.4. Optical waveguide spectroscopy

A Multiskop (Optrel, Germany) instrument was used with samples in the Kretschman prism-coupling configuration at attenuated total reflection (ATR) conditions. A p-polarized He–Ne laser (632.8 nm) was used to illuminate the prism in both TM and TE modes. Reflected light vs. angle of incidence data was converted by computer to a R vs. θ scan, $\theta = 30$–$70°$ (PS) and to 75° (PS:2BP12). BK7 glass substrates were coated with a ∼9 nm layer of chromium (to ensure gold adhesion) and a ∼30–33 nm layer of gold. A solution of 50 mg/mL PS in $CHCl_3$ was

filtered, and spincast on a gold substrate at 1000 rpm for 120 s. A solution of 50 mg/mL of 90:10 wt% PS:2BP12 in $CHCl_3$ was filtered, and spincast on the gold substrate under identical conditions. This concentration produced homogeneous films suitable for WS. Higher concentrations (e.g. 50:50 wt% PS:2BP12) gave unsuitable phase-separated films. After obtaining initial waveguide spectra, the PS:2BP12 film was irradiated ex situ for 3 h, and post-irradiation spectra were taken. Due to the necessity of moving the sample to irradiate, a sample holder was configured to hold the glass prism firmly onto the glass side of the substrate before and after irradiation. This allowed us to carefully realign the laser on the prism, and thus take waveguide spectra of the same position on the film. Three pre-irradiation and three post-irradiation waveguide spectra were taken, and averages of the simulated thickness and refractive indices are reported.

2.2.5. AFM

The surface morphologies were recorded using a PicoSPM II system (Pico Plus, Molecular Imaging) using a $10\times10\ \mu m^2$ scanner. Magnetic AC (MAC) mode was used for all images. Magnetically coated Type II MAC-levers with a spring constant of 2.8 nN/M with about 10 nm tip radius were used in the top-down configuration.

2.2.6. Contact angle

Static contact angles were measured using a CAM 200 optical contact angle meter (KSV Instruments, Ltd) with CAM 200 Software as supplied, from the same samples used for WS. A 1 μL drop of deionized water was used in all measurements. Multiple measurements were made for each substrate at various positions protected by the sample holder, as well as those exposed to UV light, to effectively give before-and-after data.

2.2.7. QCM

The QCM, crystals and the RQCM Data-Log Software (for data acquisition and monitoring) were obtained from Maxtek, Inc. A research quartz crystal microbalance (RQCM) was used to measure the oscillation frequency. Two solutions of 50 mg/mL of 90:10 and 50:50 wt% PS:2BP12 in $CHCl_3$ were filtered, and spincast at 1000 rpm for 120 s, on a polished QCM AT cut crystals (25.5 mm diameter, 5 MHz) with a Ti–Pt electrode (12.5 mm diameter). The crystals were dried overnight under vacuum at room temperature to remove all traces of solvent. For kinetics measurements, ΔFrequency was measured versus time while irradiating at ambient conditions for about 3 h, and for about 1 h after irradiation.

3. Results and discussion

For all FT-IR, IR imaging, and UV–vis work described below, a higher concentration of 2BP12 (50 mg/mL 50:50 wt% with PS: 2BP12) was used than is typical of most photodegradation studies [4,6]. Our objective in using this PS:2BP12 ratio was to ensure a significant signal attenuation within the time of observation for the BP carbonyl suitable for all FT-IR imaging, UV–vis, WS, and QCM measurements (Fig. 1(a)). Our early experiments showed that at lower amounts of 2BP12 or PS:2BP12 ratio of 90:10 wt%, all BP carbonyls was consumed within 30 min of irradiation. We judged as impractical any kinetic experiments where the reaction time is significantly shorter than the measurement time (~30 min for the imaging experiments). A second rationale for the high ratio was also to ensure and increase the occurrence of crosslinking relative to photodegradation, and to monitor these two competing processes by the techniques utilized in this study in the same time frame of observation. In the future, other compositions could be considered but would require a binary composition–property correlation plot which is beyond the reasonable scope for this study. The focus of this work is correlation of phenomena on the same time frame of observation for all measurements.

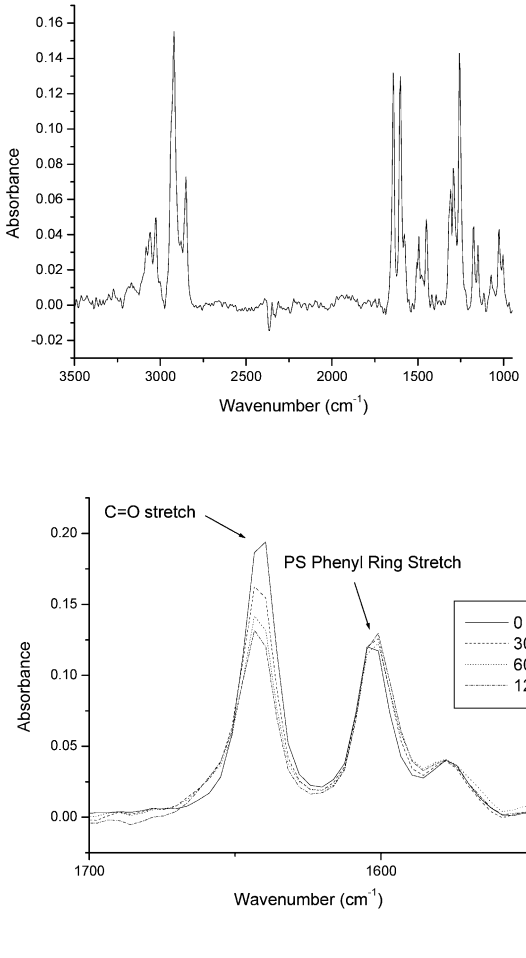

Fig. 1. FT-IR spectra of PS:2BP12 irradiated in solution and spincast onto silicon. (a) Transmission spectrum of blend prior to irradiation. (b) Decreasing 2BP12 C=O stretch (1640 cm^{-1}) with irradiation time relative to constant PS phenyl ring stretch (1601 cm^{-1}).

3.1. PS:2BP12 irradiated in solution

The ideal FT-IR imaging experiment to observe maximum crosslinking and minimum chain scission would be to irradiate PS:2BP12 in vacuo, and scan the identical region on the same film as a function of irradiation time. Due to experimental design constraints for an oxygen-free environment, we decided to irradiate a sealed, stirred PS:2BP12 solution in $CHCl_3$ to minimize exposure to oxygen, and spincast separate aliquots per irradiation time on a substrate. Although IR images could give an indication of the distribution of functional groups in each film, trends of crosslinking (and chain scission, if any) versus time might not be readily observable across separate samples. Thus, the films were observed by simple transmission IR. Since the solution was stirred to ensure homogeneity and consistent aliquot sizes were spincast, absorbance intensities should give an accurate indication of the trends sought.

As solution irradiation is continued incrementally, a continuous decrease in the C=O stretch at 1640 cm^{-1} is seen (Fig. 1(b)) up to 120 min. No new peak at ~1700 cm^{-1} is observed, where degradation carbonyls are expected. Fig. 2 shows the absorbances of the peaks at 1640 (C=O stretch), 1601 (phenyl ring stretch) and 1449 (CH_2 bend) cm^{-1}, taken relative to that at 1257 cm^{-1} (C–O stretch) and plotted versus irradiation time. A decrease is seen for the carbonyl moiety, while trends are relatively linear for the phenyl and methylene groups. This indicates that the photocrosslinking event is the major process occurring in the absence of oxygen. As described previously, the formation of conjugated double bonds does occur during vacuum irradiation, but cannot be observed in the IR due to the overlap with the phenyl ring stretch.

3.2. UV–vis spectroscopy

To verify that the polyene formation in the photodegradation could be monitored by UV–vis spectroscopy, glass slides were spincast with PS:2BP12, and irradiated over time as shown in Fig. 3 up to 180 min. The absorption

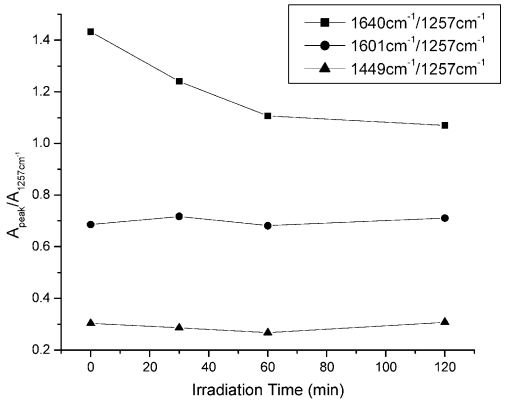

Fig. 2. Absorbances for C=O (1640 cm^{-1}), phenyl ring (1601 cm^{-1}), and CH_2 (1449 cm^{-1}) relative to C–O (1257 cm^{-1}).

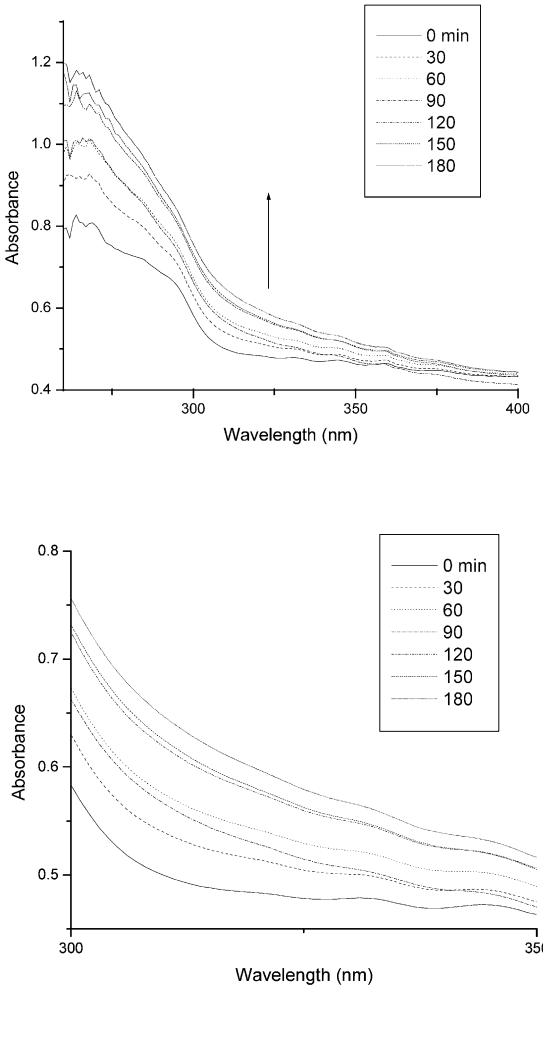

Fig. 3. UV–vis spectra of PS:2BP12. (a) Increasing absorbance at 280 nm. (b) Expanded region (300–350 nm) focusing on 310 and 340 nm.

maximum at 280 nm has been attributed to both the diene chromophore (Eq. (5), $n=2$) [9] and degradation carbonyls [28]. Longer wavelength maxima have also been reported, and assigned to polyenes of greater conjugation lengths, at 310 nm ($n=3$) and 340 nm ($n=4$) [1,28]. The latter are extremely difficult to observe as pronounced maxima, but nonetheless exhibit an increase in absorbance intensity with time (Fig. 3(b)). Thus, UV–vis is a convenient method for looking at this aspect of the PS photodegradation, i.e. conjugated C=C formation.

3.3. PS:2BP12 irradiated as thin films

Transmission FT-IR spectra (Fig. 4(a)) versus irradiation time showed an increase in intensity for a broad peak centered at ~1735 cm^{-1}, due to carbonyls that form upon PS photodegradation in the presence of atmospheric oxygen. A decrease in peak intensity at 1640 cm^{-1} also occurs, although not as rapidly as the former. A steady increase at ~3350 cm^{-1}, due to hydroperoxide production

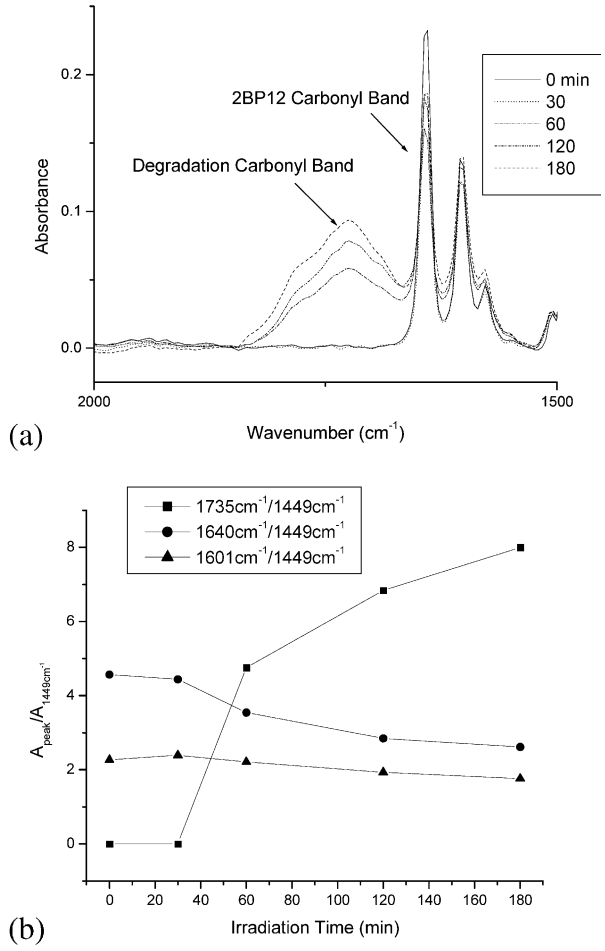

Fig. 4. (a) Increasing vs. decreasing intensities in degradation C=O (1735 cm^{-1}) and 2BP12 C=O (1640 cm^{-1}) bands, respectively. (b) Absorbances for degradation C=O, 2BP12 C=O, and PS phenyl ring stretch (1601 cm^{-1}) relative to CH_2 bend (1257 cm^{-1}).

is also observed, but has not been included in the figure. In Fig. 4(b), the absorbances of the peaks for degradation C=O, 2BP12 C=O, and PS phenyl ring stretch (1601 cm^{-1}) were taken relative to the methylene bend at 1449 cm^{-1}, and plotted versus irradiation time. Since hydroperoxides are produced, the number of C–O groups increases with time. On the other hand, Kaczmarek and co-workers have reported that polyene formation (Eq. (5)) is inhibited by benzophenone initiators relative to chain scission [6], and thus the methylene signal would be more useful to normalize the other peak absorbances. The trends in the plots above show an increase in the number of degradation carbonyls formed. The decrease in the 2BP12 carbonyls show that crosslinking occurs as a process simultaneous to photodegradation. The trend for decomposition of the phenyl ring is not as clear, but the fate of this functional group has been discussed extensively in the literature. Absorbance values at 3350 cm^{-1} were difficult to extract from the transmission spectra and were not plotted in Fig. 4(b).

The actual identity of the degradation carbonyl products has been reported as peroxy or carboxylic acids [4,9], aldehydes [4,6], aliphatic and aromatic ketones [8,9], and carboxylic esters and peresters [29]. The acetophenone end group [9,30] (1685–1690 cm^{-1}) is a particularly favored species, and is considered to be one of the species responsible for the yellowing of photodegrading PS. The new carbonyl peak in our spectra is very broad, going from ~1660 to ~1850 cm^{-1}, in excellent agreement with the data from Geetha and others [28]. Assignments of the peak in the latter work were made to ketones, aldehydes and peroxy esters (1720, 1732 and 1782 cm^{-1}, respectively). On the other hand, Otocka and co-workers [4] have described the species at 1730 cm^{-1} as either a carboxylic or peroxy acid, due to a quantitative peak shift to 1660 cm^{-1} upon exposure of the irradiated PS to concentrated ammonia vapor. We repeated their procedure on our films (exposure to NH_3 vapor for 1 h), and found nearly complete loss of the broad peak centered at 1735 cm^{-1}, and a shoulder to higher frequency of the 2BP12 C=O signal (Fig. 5(a)). Subtraction of the spectrum of irradiated PS:2BP12 from the ammonia-treated spectrum reveals the shoulder to

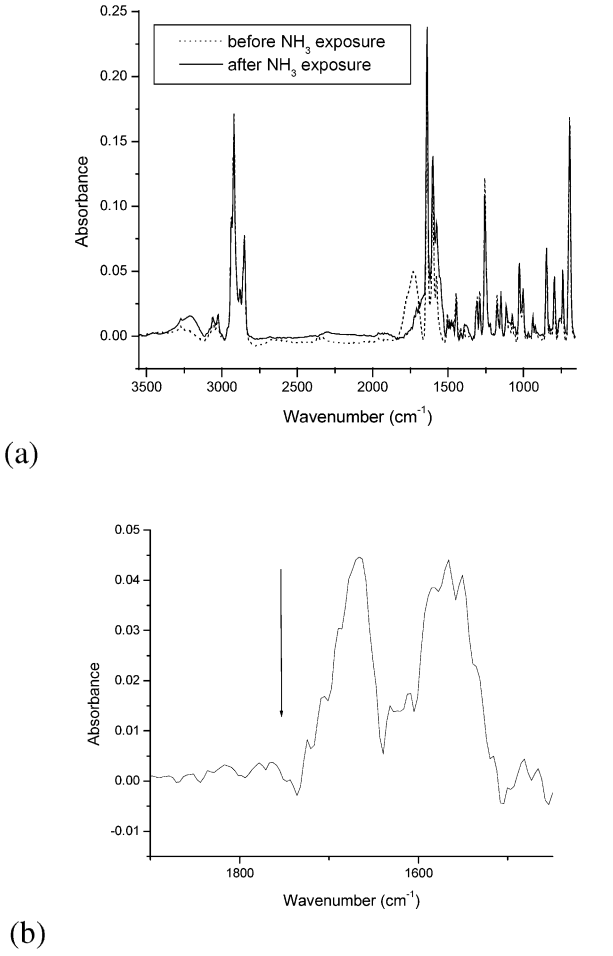

Fig. 5. (a) FT-IR spectra highlighting the loss of 1735 cm^{-1} peak upon exposure of film to ammonia vapor. (b) Carbonyl region of the subtracted spectrum from (a). Arrow points to the region formerly attributed to the amide.

be a peak at 1665 cm^{-1}, presumably due to an amide carbonyl (Fig. 5(b)).

3.4. FT-IR imaging

To our knowledge, this is the first reported use of FT-IR imaging to directly observe the photodegradation process in a PS polymer thin film system. By FT-IR imaging, it is possible to obtain 'before and after' spectral micrographs of both photodegradation and crosslinking upon UV irradiation at specific stages. For example, when small molecule photoinitiators are used, they may be readily observed by unique absorption frequencies in the IR. BP, for instance, is readily observed from the C=O stretch at ~1660 cm^{-1}. The peak is not expected to change when BP is regenerated from the singlet BP radical with formation of the hydroperoxide radical. However, crosslinking of the radical leads to the loss of the carbonyl group and a decrease in C=O peak intensity. Crosslinking in BP-modified polymers in the form of benzophenone dianhydride copolymerized with both hydrogen donor and non-donor molecules has been previously reported [20]. GPC results revealed that photocrosslinking efficiency is a nearly linear function of aliphatic hydrogen donor content in the polymer. Therefore, to facilitate the observation of both crosslinking and photodegradation in air-irradiated PS, we decided to use 2BP12, a molecule containing two BP moieties held by ether linkages to a dodecyl chain. 2BP12 should function as a more efficient crosslinker due to its bifunctional nature.

We have chosen to focus on the three pertinent wavenumbers, specifically 1640 cm^{-1} (C=O stretch, 2BP12), 1735 cm^{-1} (C=O stretch, degradation carbonyls), and 3350 cm^{-1} (O–H, hydroperoxide). All images at each wavenumber are adjusted to the same highest and lowest intensities using the IR software for maximum contrast in the changes for each functional group (Fig. 6). The images chosen at the specified irradiation times are the most illustrative of the trends in photodegradation and crosslinking in a $176 \times 176\ \mu m^2$ area of a sample (for 3D rendering, see Supporting information). These images are typical and several scans were made on different spots of the film to verify that these images are representative. The IR images provide a chemical map of both degradation and photocrosslinking processes in PS:2BP12 films where each pixel is actually equivalent to one spectra (Supporting information). An apparent orientation can be seen along the diagonal of the spectral slices from bottom left to top right. This effect may be due to a morphological ordering of the deposited material, as it is spincast on silicon. Upon irradiation, the images of the functional groups involved would be expected to roughly follow this orientation.

The changes in the IR images of the PS degradation products are more pronounced than those for the benzophenone carbonyl. This is expected as the degradation carbonyls and hydroperoxides begin from zero intensity. On the other hand, crosslinking is not expected to proceed completely, i.e. the carbonyl group at 1640 cm^{-1} would not drop to zero absorbance. This has been shown in previously-described crosslinking experiments using benzophenone-containing polymers [20]. In a film, not all benzophenone moieties are within reasonable proximity of hydrogen donors (C–H bonds). It has also been argued that hydrogen abstraction (Eq. (7)) by the ketyl radical may be reversible, and can lead to a decrease in singlet radical content without subsequent crosslinking. An important observation is that this process in not typically homogeneous as shown be the distribution intensities on the false color map. On a 32×32 pixel array or roughly an area of $176 \times 176\ \mu m^2$, the crosslinking process is not necessarily uniformly distributed. It should be noted that in FT-IR imaging it is possible to obtain the 2D spectra from each pixel of the image (Supporting information). For future practical reasons, it should be possible to investigate patterns or arrays prepared by photodegradation or photochemical crosslinking methods using FT-IR imaging.

3.5. WS, AFM, and contact angle measurements

Fig. 7 shows the changes in the WS spectra for pure PS (a) and PS:2BP12 (b) after irradiation for 180 min. Film thicknesses and refractive indices from WS simulations are also given in the figure. The refractive indices for all film directions (x, y, z planes) were equal all at any one time throughout the experiments, as expected for PS without any photo-orientable groups. No anisotropy was observed, even from the spincasting process [22]. The presence of 2BP12 did not cause any anisotropy in the film either. However, its presence affects the resulting film thickness and refractive index with irradiation. The increase in n reflects the increase in the dielectric constant ($\varepsilon = n^2$) of PS upon the introduction of polar and polarizable groups (e.g. C=O and conjugated C=C). Most polymers exhibit an increase in dielectric constant upon oxidative photodegradation.

The trends in thickness change, unlike n, are not as straightforward. At high concentrations, 2BP12 tends to phase separate from the polymer. When PS:2BP12 90:10 wt% (compared to 50:50) is used, the cloudiness and observable heterogeneity of the films are decreased enough to give meaningful WS spectra. However, the phase-incompatibility is such that as the irradiation is performed, crosslinking will be localized in the areas where 2BP12 is aggregated. Due to the inherent film dimensions, crosslinking would occur more favorably parallel to the substrate, rather than across the thickness of the film. This contraction in the former direction could result in an increase in the dimension normal to the film, and would be detected by WS as an increase in thickness. Also, chain-scission would be less pronounced in the crosslinked areas due to decreased diffusion of oxygen. On the other hand, pure PS would undergo oxidation and chain-scission, and disruption in the film surface would result in an observed decrease in thickness. These contrasting results were clearly

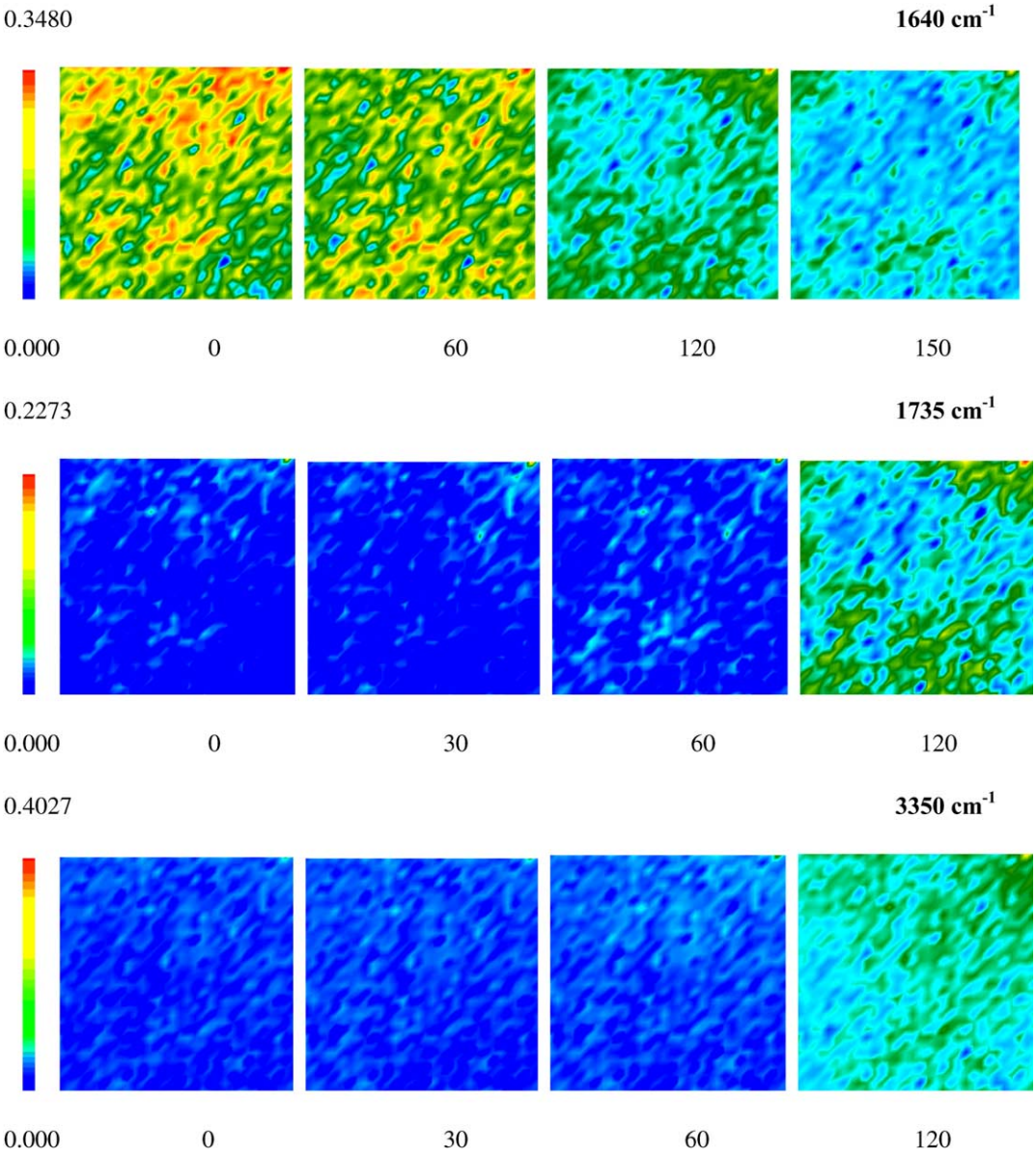

Fig. 6. FT-IR images for spectral slices extracted from 1640, 1735, and 3350 cm^{-1} as a function of irradiation time in 30 min increments. Scale bars indicate highest and lowest intensities, respectively. Area is 176×176 μm^2.

verified by the waveguide measurements and by QCM (discussed later). We have attempted to correlate the kinetics behavior of photodegradation and photocrosslinking by WS but the results have been inconclusive in terms of fit parameters (Supporting information).

Topography flattened AFM images are shown in Fig. 8, for the samples used for WS before and after irradiation. The pre-irradiation films for both pure PS and PS:2BP12 blend show smooth deposition on gold, with uniformly distributed globular features (seen as white spots in these images). After irradiation for 3 h, the globules have increased in both number and size in both samples. Post-irradiation PS shows pronounced, dark, crevice-like features through the film. On the other hand, post-irradiation PS:2BP12 shows numerous large globules up to 5 nm in diameter, while the height profile increases about 10 nm.

These AFM images are consistent with those obtained by Greenwood and co-workers [31]. They exposed six different polymer samples (including PS) to low pressure non-isothermal O_2 plasma, and observed the differences in the pre- and post-treatment surfaces by AFM and XPS. However, in our case, the presence of 2BP12 also influences the internal morphology of the film, which comprises some phase-separated domains within PS. While the experimental conditions of oxygen plasma and UV irradiation in air are obviously different, surface effects of the former include plasma oxidation, chain scission, and aggregation of the oxidized species. Thus, the net effect (if not extent) of oxidation on the surface is expected to be similar for both

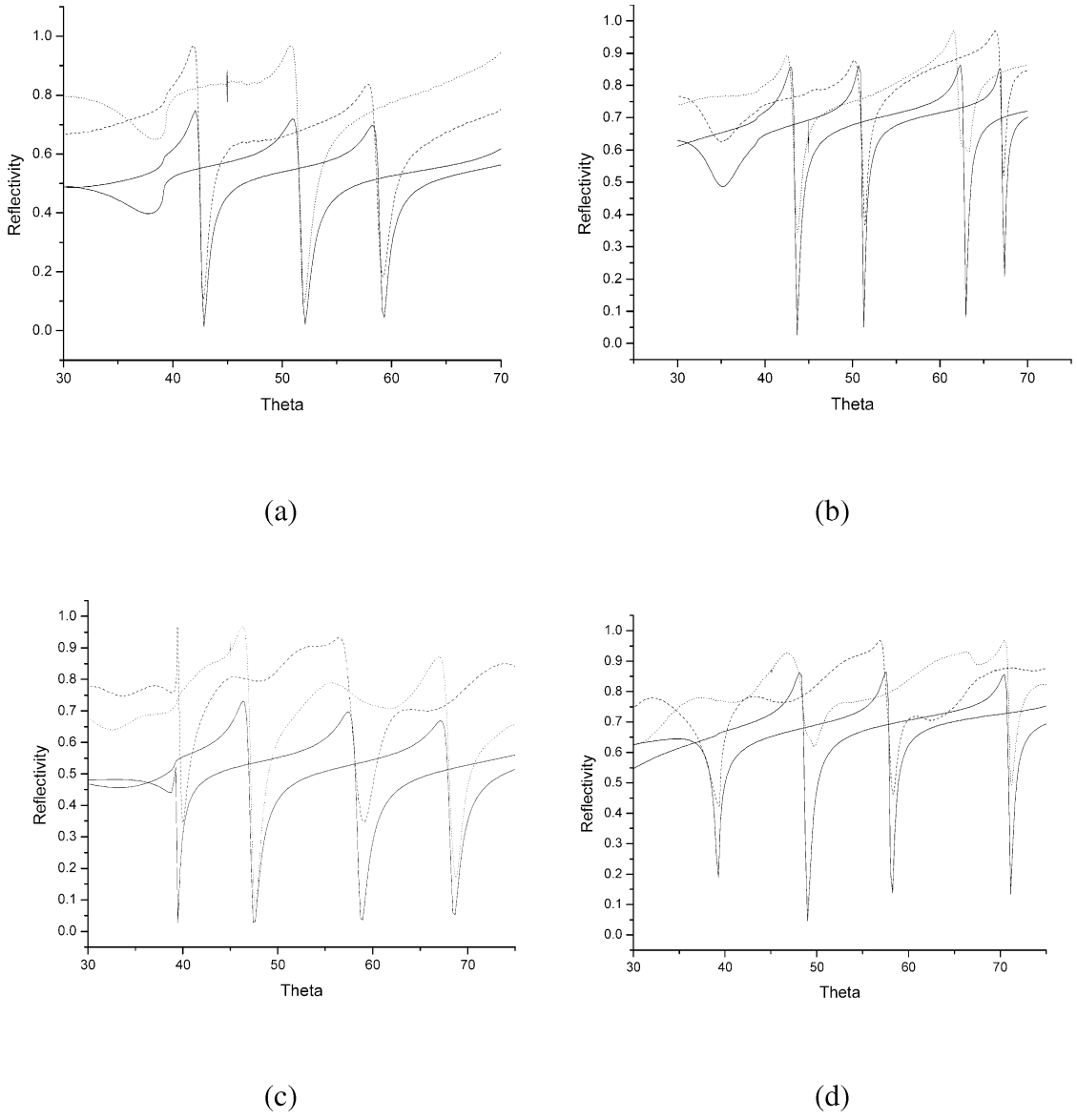

	PS, 0 min	PS, 180	PS:2BP12, 0	PS:2BP12, 180
d (nm)	1364	1327	1124	1154
n_i (i = x,y,z)	1.560	1.677	1.587	1.670

Fig. 7. (a) TM (p-polarization) and (b) TE (s-polarization) modes for PS. (c) TM (p-polarization) and (d) TE (s-polarization) modes for PS:2BP12. Dashed and dotted curves are spectra at 0 and 180 min irradiation time, respectively. Solid curves are best experimental fits from Fresnel calculations. Included table summarizes results for thicknesses and refractive indices.

techniques. Their pre-plasma AFM images of PS show even distributions of hemispherical features, effects due to the film casting methods used. Post-plasma images of all polymers studied exhibit a highly globular surface, attributed to agglomeration of lower-molecular weight oxidation and chain scission products. Interestingly, an inverse correlation is seen between the degree of oxidation (from Δ O:C data by XPS) and mean globule size. Assuming that these O_2 plasma treatment AFM data parallel those we obtained with photodegradation in air, both WS and AFM results show that PS alone is more extensively oxidized compared to PS:2BP12 under identical conditions.

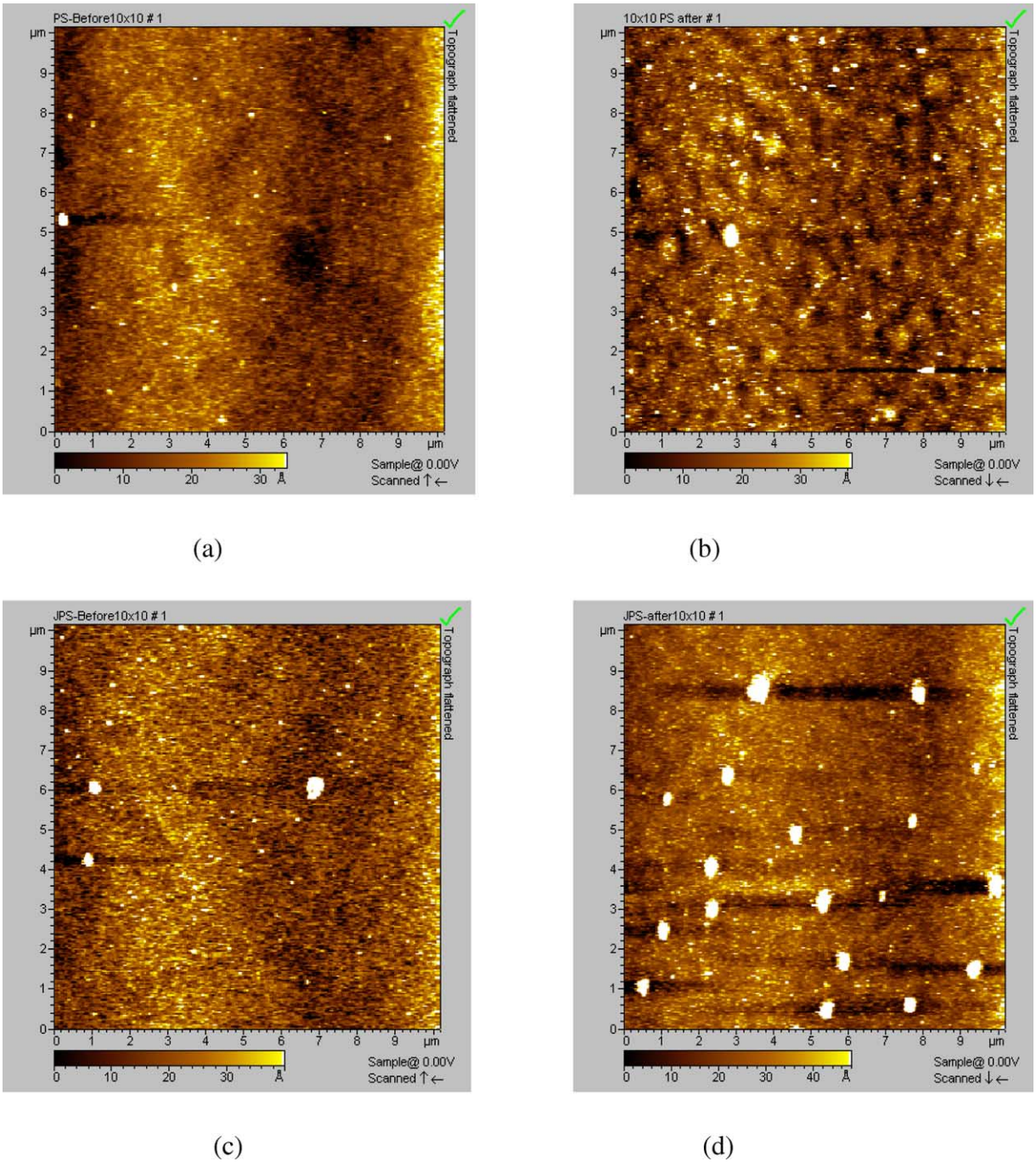

Fig. 8. Topography flattened AFM Images for: (a) pre-irradiation PS, (b) post-irradiation PS, (c) pre-irradiation PS:2BP12, and (d) post-irradiation PS:2BP12.

While 2BP12 in minimal amounts may initiate and increase PS photodegradation, the relatively high concentration used is in this regime causes the crosslinking pathway to become more dominant. Thus, the smaller globules in post-irradiation PS indicate a greater degree of oxidation, and the crevices observed point to more extensive chain scission on the surface, relative to a PS:2BP12 blend.

A surface energy analysis of our samples on gold was performed using static contact angle measurements, with the results presented in the table below. The PS film gave average values of 93 and 48°, for non-irradiated and irradiated samples, respectively. The contacts angles for the PS:2BP12 sample showed a change from 88 to 44°. The small difference in values in the irradiated areas for both samples (48 vs. 44°) does not effectively reflect the variation in extent of oxidation of the samples shown by WS and AFM. Each sample also exhibited relatively large ranges (± 5) in contact angle at different spots, due to both variations in film homogeneity and non-uniform photodegradation in the exposed portions. However, the decrease in

θ in non-irradiated versus irradiated samples is entirely consistent with the introduction of highly polar groups (hydroperoxides and carbonyls) and decreased hydrophobicity.

3.6. QCM

The negative sign in Eq. (13) indicates that as mass is adsorbed during the irradiation process, a decrease in frequency should be observed versus time. This is the trend observed for the ΔF vs. time data (Fig. 9(a)), except for a sudden rise in ΔF when the irradiation lamp was first turned on. The frequency steadily decreased for about 200 min, after which the irradiation was stopped. A sudden rise is again observed, then a steep drop, after which a leveling off is finally observed.

Δm vs. time plots are shown in Fig. 9(b) for both 90:10 and 50:50 wt% PS:2BP12. The positive ΔF (negative Δm) upon turning on the UV lamp is caused by an increase in the temperature of the quartz crystal. Separate measurements using the lamp at the same distance and power settings indicated an increase from 28 °C to an average of 31 °C. The oscillating frequency of a QCM crystal increases linearly with temperature, and frequency drifts can be observed with changes as small as a fraction of a degree [32]. The marked QCM response during irradiation is due to fluctuations in the lamp power output, and therefore, the temperature of the crystal. This is shown by the drop in frequency (increase in Δm) when lamp was turned off and the relatively smooth signal as the crystal cooled to ambient temperature.

QCM is thus an effective monitor for oxygen uptake as decomposition occurs, leading to the formation of hydroperoxides and carbonyl products. During PS photodegradation, carbon dioxide and water are also lost [30]. However, quantum yields for oxygen absorption (600 Torr), carbon dioxide formation, and water formation have been reported as 2.7×10^{-2}, 8.3×10^{-3}, and 9.5×10^{-3}, respectively [9]. Thus, a net increase in mass in irradiated PS occurs, and is readily observed by this technique. It is notable that while they follow similar trends, the plot for the 50:50 blend gives lower mass increases compared to that for the 90:10. This is consistent with the higher 2BP12 concentration causing increased crosslinking (with no oxygen uptake) relative to photodegradation.

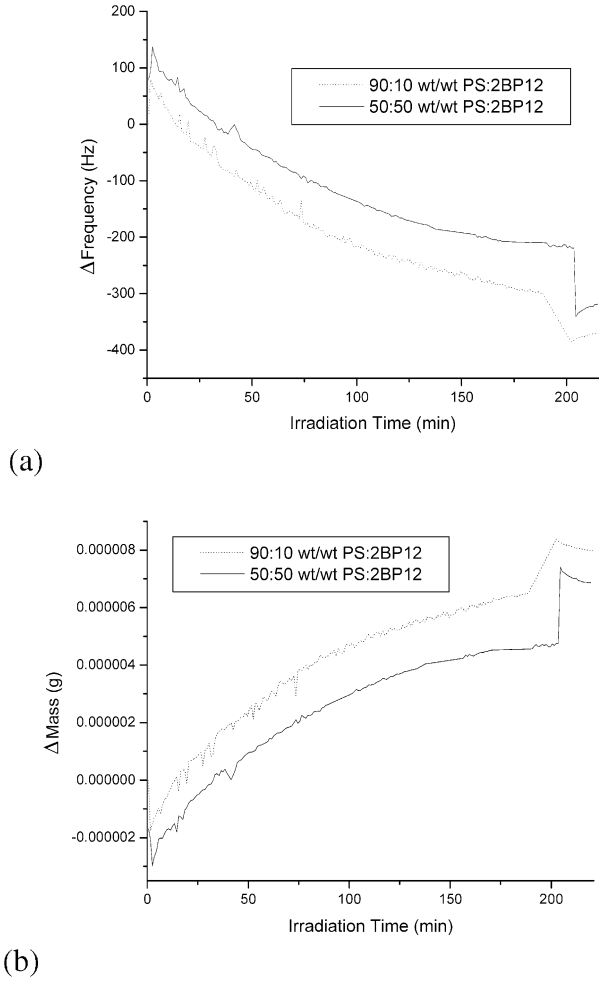

Fig. 9. QCM plots for (a) ΔFrequency (Hz) and (b) ΔMass (g) as a function of irradiation time.

4. Conclusions

In this work, we have investigated systematically the photodegradation and photocrosslinking of benzophenone modified PS thin films. While there are myriad techniques for the physico–chemical analysis of photodegradation and photocrosslinking in the bulk, relatively fewer spectroscopic and microscopic methods have been combined and applied to polymer thin films within the same time frame of observation. Since the oxidation and chain scission processes occur only within a limited distance (100s to 1000s of nm) from the surface, chemical and physical properties at or near this surface become increasingly important. By adding an amount of 2BP12 greater than is typically used for photoinitiators in literature, both extensive crosslinking and photodegradation were easily observed for the spectral, optical, and acoustic investigation methods. FT-IR imaging effectively shows consistent trends in functional group intensities, in the 2BP12 carbonyl, as well as for carbonyl and hydroperoxides degradation products. Refractive index changes consistent with production of polar groups on the surface are observed using evanescent waveguide spectroscopy. The presence of such polar groups on the surface is further verified by static water contact angle measurements. The thickness variations seen in WS depend on whether photodegradation (pure PS) or crosslinking (with PS:2BP12) is the dominant reaction on the surface. Our before-and-after AFM images on the same samples confirm our WS data. Finally, the kinetics of oxygen uptake in the nanogram scale versus time can easily be monitored using mass (and resonance frequency) changes in QCM. Thus, the simultaneous crosslinking and

photodegradation trends can be quantitatively determined based on correlation of the IR, UV–vis, WS, and QCM measurements since all of the data obtained were within the same time frame of observation. The percentage differences (before and after) or time correlation plots (kinetics) can be used to prepare a more quantitative picture of composition–property or structure–property relationships in the future. The use of these combined techniques can also be extended to the analysis of any number of polymeric thin film systems undergoing other types of degradation and reactive processes. Studies are underway to investigate in situ patterning processes in polymer thin films.

Acknowledgements

We acknowledge partial financial support from NSF-CTS (0330127) and DMR-0315565. We would also like to acknowledge technical support from Molecular Imaging Inc., Maxtek Inc., and Optrel GmBH.

Supplementary data

Supplementary data associated with this article can be found at doi:10.1016/j.polymer.2005.05.050

References

[1] Rabek JF. Polymer photodegradation: mechanism and experimental methods. Cambridge: Chapman & Hall; 1995, p. 185–217.
[2] Grassie N, Weir WA. J Appl Polym Sci 1965;9:987–98.
[3] The following is a list of representative publications and is by no means exhaustive: (a) Achhammer BG, Reiney MJ, Wall LA, Reinhart FW. J Polym Sci 1952;8:555–71.
(b) Reiney MJ, Tyron J, Achhammer BG. J Res Natl Bur Stand 1953; 51:155–61.
(c) Grassie N, Weir NA. J Appl Polym Sci 1965;9:963–74 [see also p. 975–86; 999–1003].
(d) Ranby B, Rabek JF. Photodegradation, photooxidation and photostablization of polymers: principles and applications. New York: Wiley; 1975, p. 165–184.
(e) Weir NA. Eur Polym J 1978;14:9–14.
(f) Weir NA. J Polym Sci, Polym Chem Ed 1978;13–31:1123–36.
(g) Lucas PC, Porter RS. Macromolecules 1994;27:3666–8.
[4] (a) Otocka EP, Curran S, Porter RS. J Appl Polym Sci 1983;28:3227–33.
(b) Tamai T, Hashida I, Ichinose N, Kawanishi S, Inoue H, Mizuno K. Polymer 1996;37:5525–8.
[5] Gueskens G, Bastin P, Lu-Vinh Q, Rens M. Polym Degrad Stab 1981; 3:295–306.
[6] Kaczmarek H, Kaminska A, Swiatek M, Sanyal S. Eur Polym J 2000; 36:1167–73.
[7] Kubica J, Waligora B. Eur Polym J 1977;13:325–9.
[8] Torikai A, Takeuchi T, Fueki K. Polym Photochem 1983;3:307–20. Scherzer T, Tauber A, Mehnert R. Vib Spectrosc 2002;29:125–31.
[9] Gueskens G, Baeyens-Volant D, Delaunois G, Lu-Vinh Q, Piret W, David C. Eur Polym J 1978;14:291–7.
[10] Tanaka K, Takahara A, Kajiyama T. Macromolecules 1997;30:6626.
[11] Tawa K, Knoll W. Macromolecules 2002;35:7018–23.
[12] (a) Koenig JL, Wang S-Q, Bhargava R. Anal Chem A-Pages 2001; 73:360A–39.
(b) Colarusso P, Kidder LH, Levin IW, Fraser JC, Arens JF, Lewis EN. Appl Spectrosc 1998;52:106A–120.
(c) Bhargava R, Levin IW. Anal Chem 2001;73(21):5157–67.
[13] Li G-Y, Koenig JL. Appl Spectrosc 2002;56:1390–6.
[14] Rafferty DW, Koenig JL, Magyar G, West JL. Appl Spectrosc 2002; 56:1549–51.
[15] Gupper A, Chan KLA, Kazarian SG. Macromolecules 2004;37(17): 6498–503.
[16] Gupper A, Wilhelm P, Schmied M, Kazarian SG, Chan KLA, Reussner J. Appl Spectrosc 2002;56:1515–23.
[17] Miller-Chou BA, Koenig JL. Macromolecules 2003;36:4851–61.
[18] Kazarian SG, Chan KLA. Macromolecules 2004;37:579–84.
[19] (a) Ellis G, Marco C, Gomez M. Infrared Phys Technol 2004;45(5–6):349–64.
(b) Dumas P, Tobin MJ. Spectrosc Eur 2003;15(6):17–23.
(c) Otts DB, Zhang P, Urban MW. Langmuir 2002;18:6473–7.
(d) Chan KLA, Kazarian SG, Mavraki A, Williams DR. Appl Spectrosc 2005;59(2):149–55.
[20] Lin AA, Sastri VR, Tesoro G, Reiser A, Eachus R. Macromolecules 1988;2:1165–9.
[21] Knoll W. Annu Rev Phys Chem 1998;49:569–638.
[22] Patton D, Park M, Wang S, Advincula RC. Langmuir 2002;18: 1688–94.
[23] Lau KHA, Tan L-S, Tamada K, Sander MS, Knoll W. J Phys Chem B 2004;108:10812–8.
[24] Okahata Y, En-na G, Ebato H. Anal Chem 1990;62:1431–8.
[25] Sauerbrey G. Z Phys 1959;155:206–22.
[26] Baba A, Kaneko F, Advincula RC. Colloids Surf A 2000;173: 39–49.
[27] Fan X, Zou Q, Xia C, Cristofoli W, Mays J, Advincula R. Langmuir 2002;18:4511–8.
[28] Geetha R, Torikai A, Nagaya S, Fueki K. Polym Degrad Stab 1987;9: 279–92.
[29] Khalil Z, Michaille S, Lemaire J. Makromol Chem 1987;188: 1743–56.
[30] Grassie N, Weir WA. J Appl Polym Sci 1965;9:987–98.
[31] Greenwood OD, Hopkins J, Badyal JPS. Macromolecules 1997;30: 1091–8.
[32] Snook G. Investigation of solid-state reactions by electrochemical and quartz crystal microbalance measurements. Doctoral Dissertation, Monash University; 2000.